REPORT SSD-TR-90-31

(4)

Direct Observation of NF(X) Using Laser-Induced Fluorescence: Kinetics of the $NF^3\Sigma^-$ Ground State

Prepared by

R. F. HEIDNER III, J. S. HOLLOWAY, H. HELVAJIAN, AND J. B. KOFFEND
Aerophysics Laboratory
Laboratory Operations
The Aerospace Corporation
El Segundo, CA 90245–4691

6 August 1990

Prepared for

SPACE SYSTEMS DIVISION
AIR FORCE SYSTEMS COMMAND
Los Angeles Air Force Base
P.O. Box 92960
Los Angeles, CA 90009–2960

This report was submitted by The Aerospace Corporation, El Segundo, CA 90245-4691, under Contract No. F04701-88-C-0089 with the Space Systems Division, P. O. Box 92960, Los Angeles, CA 90009-2960. It was reviewed and approved for The Aerospace Corporation by R. W. Fillers, Director, Aerophysics Laboratory. Capt. R. Riviere was the project officer for the Mission-Oriented Investigation and Experimentation (MOIE) Program.

This report has been reviewed by the Public Affairs Office (PAS) and is releasable to the National Technical Information Service (NTIS). At NTIS, it will be available to the general public, including foreign nationals.

This technical report has been reviewed and is approved for publication. Publication of this report does not constitute Air Force approval of the report's findings or conclusions. It is published only for the exchange and stimulation of ideas.

RAFAEL A. RIVIERE, Capt, USAF
MOIE Project Officer
SSD/CNL

JOHATHAN M. EMMES, Maj, USAF
MOIE Program Manager
AFSTC/WCO OL-AB

REPORT DOCUMENTATION PAGE

1a. REPORT SECURITY CLASSIFICATION Unclassified	1b. RESTRICTIVE MARKINGS
2a. SECURITY CLASSIFICATION AUTHORITY	3. DISTRIBUTION/AVAILABILITY OF REPORT Approved for public release; distribution unlimited
2b. DECLASSIFICATION/DOWNGRADING SCHEDULE	
4. PERFORMING ORGANIZATION REPORT NUMBER(S) TR-0090(5930-04)-3	5. MONITORING ORGANIZATION REPORT NUMBER(S) SSD-TR-90-31
6a. NAME OF PERFORMING ORGANIZATION The Aerospace Corporation Laboratory Operations 6b. OFFICE SYMBOL *(If applicable)*	7a. NAME OF MONITORING ORGANIZATION Space Systems Division
6c. ADDRESS *(City, State, and ZIP Code)* El Segundo, CA 90245-4691	7b. ADDRESS *(City, State, and ZIP Code)* Los Angeles Air Force Base Los Angeles, CA 90009-2960
8a. NAME OF FUNDING/SPONSORING ORGANIZATION 8b. OFFICE SYMBOL *(If applicable)*	9. PROCUREMENT INSTRUMENT IDENTIFICATION NUMBER F04701-88-C-0089
8c. ADDRESS *(City, State, and ZIP Code)*	10. SOURCE OF FUNDING NUMBERS PROGRAM ELEMENT NO. / PROJECT NO. / TASK NO. / WORK UNIT ACCESSION NO.

11. TITLE *(Include Security Classification)*

Direct Observation of NF(X) Using Laser-Induced Fluorescence: Kinetics of the $NF^3\Sigma^-$ Ground State

12. PERSONAL AUTHOR(S)

Heidner III, Raymond F.; Holloway, John S.; Helvajian, Henry; and Koffend, John B.

13a. TYPE OF REPORT	13b. TIME COVERED	14. DATE OF REPORT *(Year, Month, Day)*	15. PAGE COUNT
	FROM _____ TO _____	1990 August 6	30

16. SUPPLEMENTARY NOTATION

17. COSATI CODES		
FIELD	GROUP	SUB-GROUP

18. SUBJECT TERMS *(Continue on reverse if necessary and identify by block number)*

Nitrogen fluoride
Nitrogen difluoride
Vibrational relaxation
Rotational relaxation
UV photolysis

19. ABSTRACT *(Continue on reverse if necessary and identify by block number)*

The gas phase kinetics of the $NF(X^3\Sigma^-)$ ground state radical have been investigated by direct observation. $NF(X^3\Sigma^-)$ was produced from the KrF laser photolysis of NF_2 and was directly monitored in the gas phase using laser-induced fluorescence (LIF) via the NF $b^1\Sigma - X^3\Sigma^-$ transition. The extremely hot nascent $NF(X^3\Sigma^-)$vibrational distribution (T_{vib} = 2350 K) was exploited to investigate vibrational relaxation with CO_2 and SF_6. While CO_2 proved to be inefficient for NF(X) vibrational relaxation ($k_{1-0} = 3.7 \times 10^{-14}$ cm^3/molecule-sec), SF_6 is a rapid quencher ($k_{1-0} = 1.2 \times 10^{-12}$ cm^3/molecule-sec). Information on rotational relaxation of $NF(X^3\Sigma^-)$ was also obtained. The NF ground state is seen to be removed by reaction with NF_2 with a surprisingly large efficiency ($k = 2.0 \times 10^{-12}$ cm^3/molecule-sec). The NF(X) + NF(X) → N_2 + 2F rate coefficient is estimated to be < 5×10^{-12} cm^3/molecule-sec.

20. DISTRIBUTION/AVAILABILITY OF ABSTRACT	21. ABSTRACT SECURITY CLASSIFICATION
☒ UNCLASSIFIED/UNLIMITED ☐ SAME AS RPT. ☐ DTIC USERS	Unclassified
22a. NAME OF RESPONSIBLE INDIVIDUAL	22b. TELEPHONE *(Include Area Code)* / 22c. OFFICE SYMBOL

PREFACE

This work was supported by the Air Force Weapons Laboratory under Air Force Space Systems Division (SSD) Contract F04701-88-C-0089.

CONTENTS

FIGURES

TABLES

I. INTRODUCTION

Reactions that involve NF_2 and NF are of interest since many of them produce electronically excited products. In particular, the H_2/NF_2 system[1] serves as a source of metastable $NF(a^1\Delta)$ which forms the basis for several proposed visible chemical lasers.[2-4] The H_2/NF_2 reaction system has been the subject of several studies where particular attention has been paid to the formation of energetic species.[5-8] The reaction kinetics of the $NF(X^3\Sigma^-)$ radical and its ultimate fate are critical to a full understanding of this system since it is the principal source of F atoms which propagate the overall chain reaction.

The NF ground state has previously been detected using infrared absorption spectroscopy in both the gas phase[9] and in rare gas matrices.[10] Laser-induced fluorescence has also been used to investigate the radiative decay of the NF(a) and NF(b) states in solid argon.[11] There have been several studies[2,5,6] of NF radical reactions with various transient species which include H and N atoms in addition to NF itself. Apart from recent NF(a,b) electronic quenching measurements,[8,12-14] there have been no prior studies on the state-specific kinetics of the NF molecule.

Both $NF(a^1\Delta)$ and $NF(X^3\Sigma^-)$ are energetically accessible from the 249 nm photolysis of NF_2 and are produced in 10% and 90% yields, respectively.[8,15] The $NF(X^3\Sigma^-)$ photofragment is born with a high degree of rotational and vibrational excitation.[16] We have taken advantage of this excited $NF(X^3\Sigma^-)$ nascent population distribution to perform vibrational and rotational kinetic measurements on the NF ground state. Gas phase LIF of NF via the b-X transition was employed to directly probe specific vibrational levels and to determine their time behavior.

II. EXPERIMENTAL

A Lumonics 400 Hyperex excimer laser operating with KrF (249 nm) was used as a source of $NF(X^3\Sigma^-)$ via the photolysis of NF_2, which produces $NF(X^3\Sigma^-)$ in high yield. The photolysis laser light passed through a series of beam shaping lenses into a heated photolysis cell. A MgF_2 entrance window prevented fluorine etching, which would have occurred if a Suprasil window were used. Two slit apertures were placed in the beam path to suppress scattered excimer light. A portion of the KrF laser radiation was reflected into a Laser Precision RJP-734 power meter using an uncoated Suprasil window. Tunable probe laser light from a Quantel Datachrome 581C Nd-YAG pumped dye laser system, operating with Coumarin 500 dye, crossed the KrF laser beam in the observation region at the center of the cell. A small fraction of the dye laser radiation was monitored with a silicon photodiode to provide relative power measurements. The wavelength of the probe laser was determined using a Lasertechnics model 100F Fizeau wavemeter. A diagram of the experimental arrangement is shown in Fig 1.

The gases in these experiments used without further purification were CO_2 (Matheson 99.99%), Ar (Matheson 99.99%), SF_6 (MG Gases 99.9%), and N_2F_4 (Hercules 96%). Mixtures of N_2F_4 in argon were prepared and stored at 100 psia in a stainless steel reservoir. Reagents were flowed through calibrated Tylan flowmeters into the multi-axis photolysis cell. The cell, constructed of stainless steel and Teflon coated internally to minimize wall reactions, was wrapped in heating tape and maintained at 144°C. At this temperature, the N_2F_4 is >95% dissociated into NF_2 for the NF_2 densities used in these experiments.[17-21] Cell pressure was measured with an MKS Baratron capacitance manometer.

A gatable EMI 9816QB photomultiplier tube equipped with a 20 nm bandwidth interference filter centered at 550 nm and a 5 cm focal length lens was mounted on one arm of the photolysis cell to view the NF b-X LIF signal through a Suprasil window. The PMT gate was turned on 180 μsec (τ_{rad} b-X = 23 msec)[2] after the b-X probe pulse in order to eliminate scattered dye

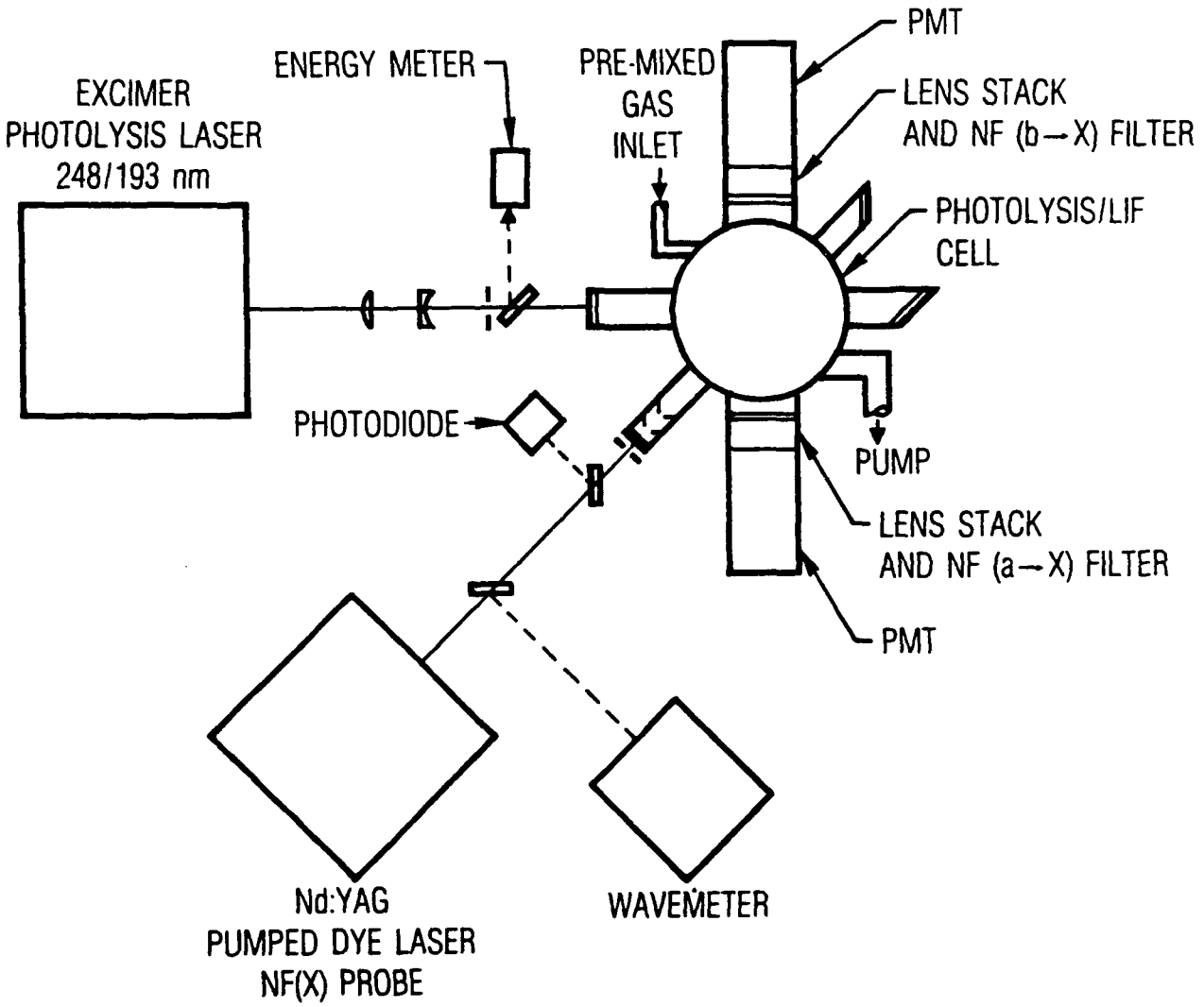

Fig. 1. Diagram of the Experimental Apparatus

laser light. Since the strong NF b-X vibronic bands are diagonal in vibrational quantum number[22,23] (q_{00}=0.96),[1] use of a gated PMT was essential for these experiments. The timing sequence used to obtain NF($X^3\Sigma^-$) time profiles is described as follows. The excimer laser is operated at a repetition rate of 10 Hz while the dye laser is pulsed at a rate of 5 Hz, synchronized to fire upon every other KrF shot. The PMT output, amplified with a Tektronix model AM-502 amplifier, is processed using two channels of an SRS model SR250 boxcar integrator. One channel of the boxcar, triggered in phase with the dye laser at 5 Hz, obtains the LIF signal. The second channel, which is triggered out of phase with the probe laser, acquires any signal not associated with the dye laser. This dual channel arrangement was necessary in order to record the background for eventual subtraction. The background is primarily due to long-lived cell window fluorescence caused by scattered excimer laser radiation in addition to NF b-X emission from the NF_2 photolysis.[8] The delay between the excimer laser photolysis and the dye laser probe pulses was scanned using an SRS model SR200 gate scanner, whose output was used to trigger the excimer laser. The magnitude of the scan width was as short as 1 μsec to as long as 300 μsec, depending upon the kinetic process under study. A third boxcar integrator was used to record the relative dye laser power, obtained from the silicon photodiode. The outputs from the three boxcars, along with the analog output from the excimer laser power meter, were digitized and stored with a DEC 11/73 laboratory computer.

III. RESULTS AND DISCUSSION

A. $NF(X^3\Sigma^-)$ VIBRATIONAL RELAXATION

Photolysis of NF_2 at 249 nm results in an extremely "hot" $NF(X^3\Sigma^-)$ vibrational distribution. An excitation spectrum from the KrF photolysis of 0.27 Torr NF_2 in 0.75 Torr Ar is depicted in Fig. 2. The spectrum was recorded using a fixed delay of 15 μsec between the KrF photolysis laser and the dye laser probe. A simulation of the spectrum is also presented in Fig. 2. There is good agreement between the experimental data and the simulation, calculated using an NF ground state rotational temperature of 420 K and a vibrational temperature of 2350 K. It should be noted that the rotational distribution is relaxed to our operating temperature. However, since Ar is very inefficient for $NF(X^3\Sigma^-)$ vibrational relaxation, the spectrum in Fig. 2 reflects the $NF(X^3\Sigma^-)$ nascent vibrational distribution. We took advantage of this excited distribution to investigate the vibrational relaxation kinetics for several $NF(X^3\Sigma^-)$ levels with CO_2 and SF_6. The time behavior for selected NF ground state vibrational levels was obtained by tuning the probe laser to a particular $b^1\Sigma(v', N')$-$X^3\Sigma^-(v'',N'')$ transition and recording the LIF as a function of the delay between the KrF laser and the dye laser.

NF $X^3\Sigma^-(v'', N'')$ time behavior traces were fit to a double exponential function of the form $A_1\exp(-A_2t) - A_3\exp(-A_4t)$. A typical experimental trace and fit to the data from the photolysis of 0.26 Torr NF_2 in 10 Torr SF_6 is presented in Fig. 3. Figure 4 depicts a plot of the decay of $NF(X)^3\Sigma^-$ ($v''=2$, $N''=9$) with SF_6 density. The nonzero intercept at $[SF_6]=0$ is due to removal by the parent molecule and is discussed below. Similar plots for formation and decay rates were obtained for other NF(X) vibrational levels studied, and the results for SF_6 and CO_2 are summarized in Table 1.

The NF ground state vibrational spacing[22] is 1141 cm^{-1}, corresponding to nearly 4 kT at our 420 K operating temperature. Thus one expects that nearly all of the collisions of $NF(v''>0)$ with the buffer gas result in

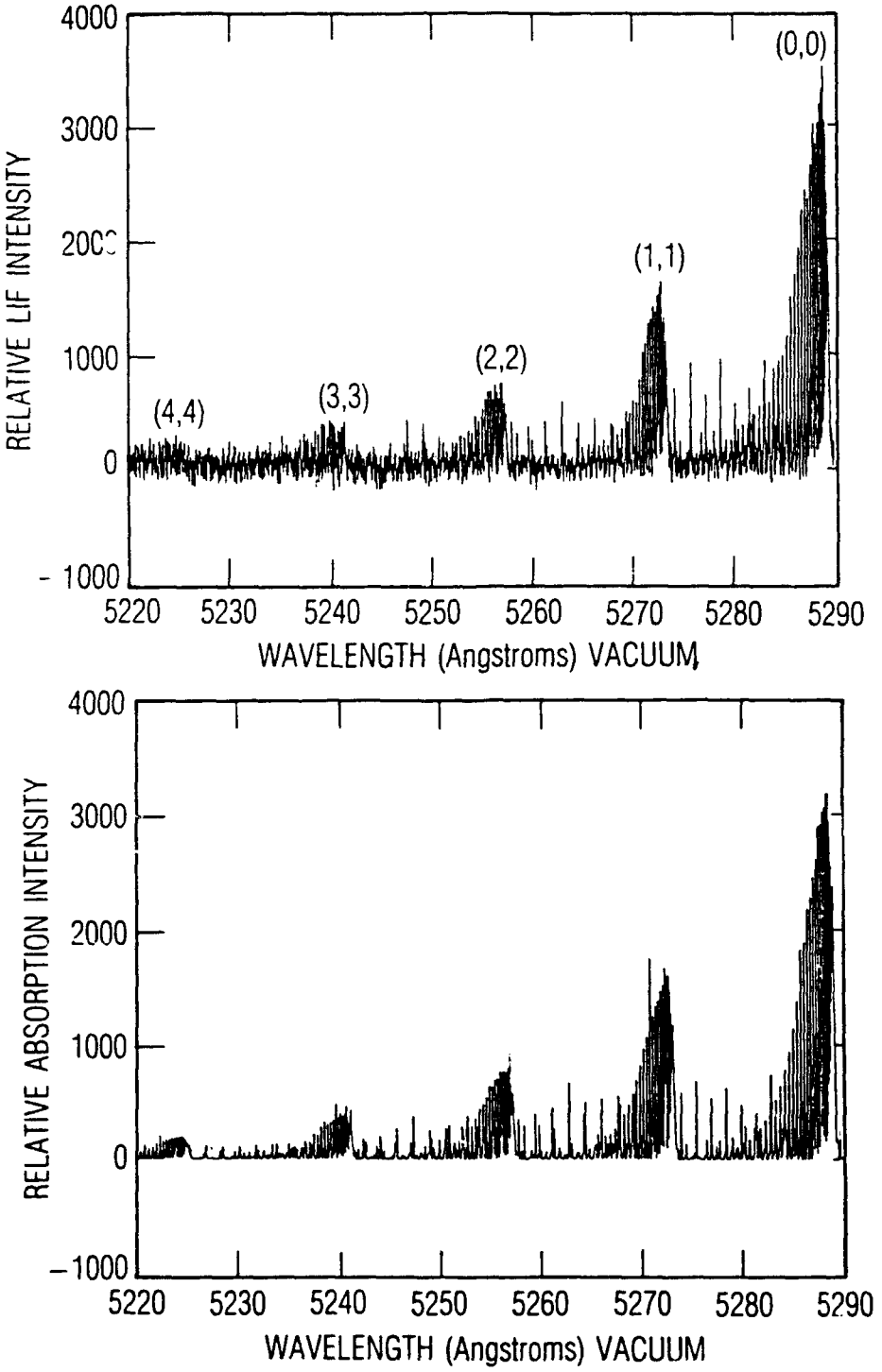

Fig. 2. Upper Trace: NF b-X Excitation Spectrum Taken from the KrF Photolysis of 0.27 Torr NF_2 in 0.75 Torr Ar. A delay of 15 μsec between the KrF laser and the dye laser was used. Lower Trace: Calculated Spectrum Using Molecular Constants of Ref. 17. A vibrational temperature of 2350 K and a rotational temperature of 420 K were used.

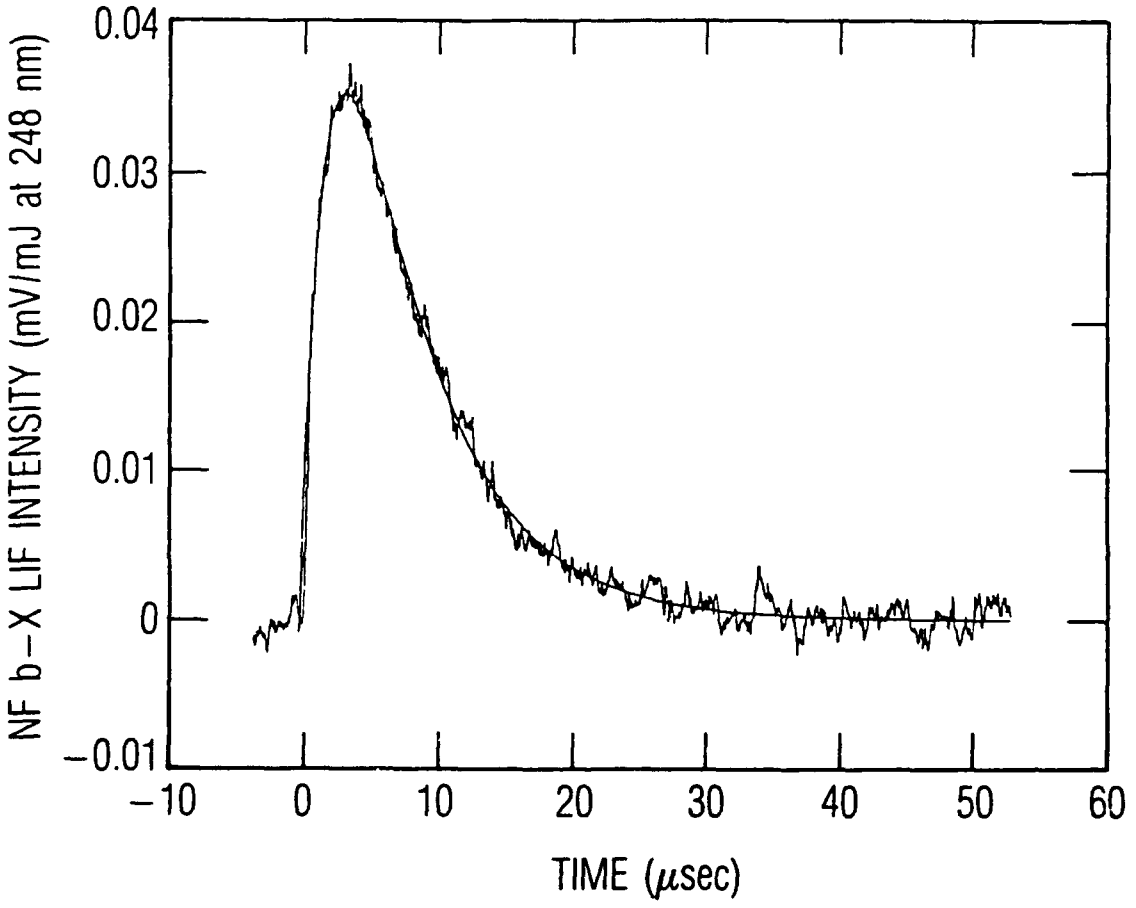

Fig. 3. Time Profile of the v"=2, N"=9 Level of NF(X). The abscissa represents the time between the KrF photolysis pulse and the dye laser probe pulse. Partial pressures of NF_2, SF_6, and Ar are 0.26, 1.1, and 1.2 Torr, respectively. A double exponential fit to the data is also shown.

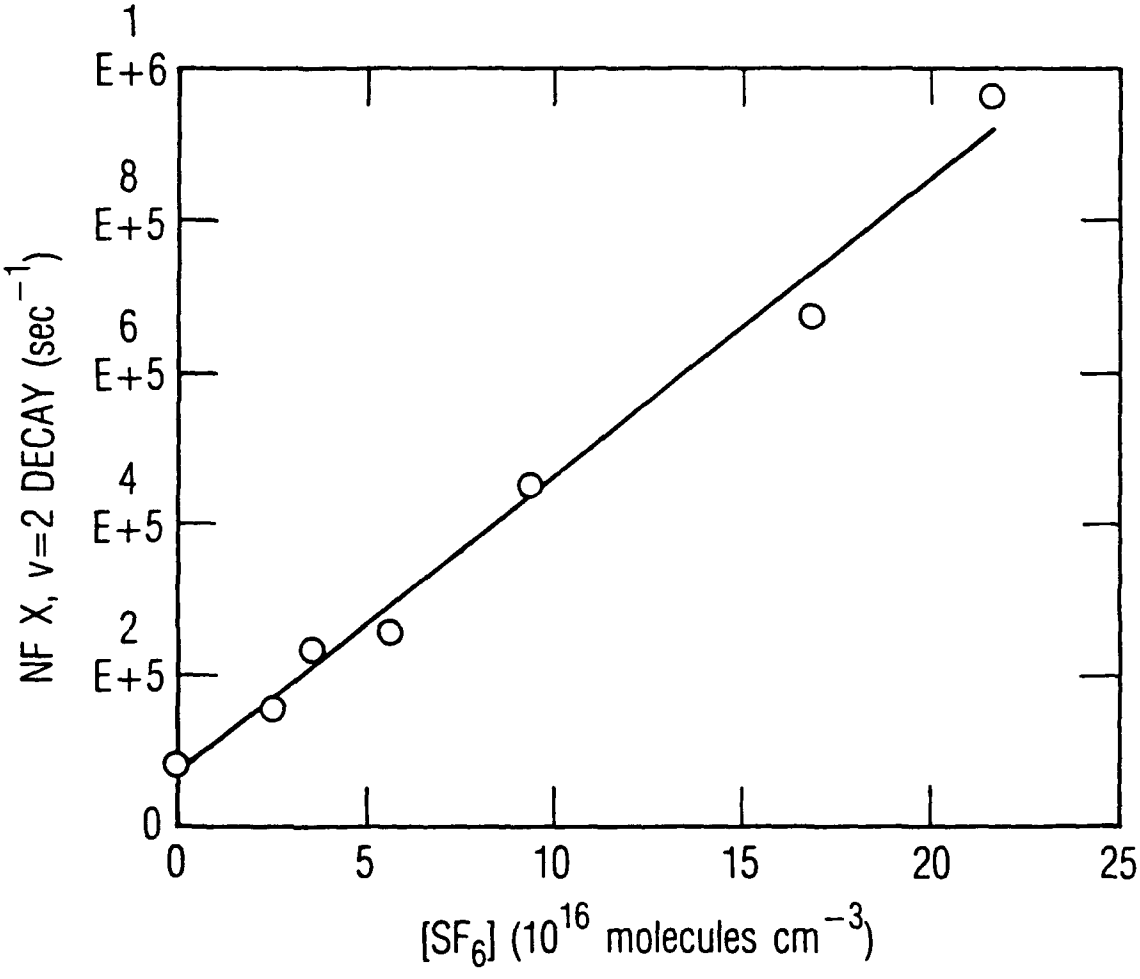

Fig. 4. Decay Rate of NF(X), v"=2. N"=9 Plotted vs SF_6 Density. The circles are the experimental data and the solid line is a linear fit whose slope is 3.9×19^{-2} cm^3/molecule-sec.

Table 1. NF Ground State Vibrational Relaxation Rate Constants[a]

v″	Formation Rate	Decay Rate
	CO_2	
0	$4.5(1.0) \times 10^{-14}$	
1	$6.5(2.0) \times 10^{-14}$	$3.7(1.0) \times 10^{-14}$
2	$1.2(0.4) \times 10^{-13}$	$7.5(2.0) \times 10^{-14}$
	SF_6	
0	$1.41(0.30) \times 10^{-12}$	
1	$3.05(0.60) \times 10^{-12}$	$1.21(0.25) \times 10^{-12}$
2	$9.50(1.80) \times 10^{-12}$	$3.92(0.80) \times 10^{-12}$

[a]All rate constants have units cm^3/molecule-sec. Estimated uncertainties (2σ) given in parentheses.

vibrational quenching rather than in vibrational excitation. Under the assumption that multi-quanta processes have low probability, we expect that the $NF(X^3\Sigma^-)$ vibrational manifold will not be strongly coupled at our operating temperature and that the rate coefficients listed in Table 1 closely approximate state-to-state vibrational relaxation rate constants. To provide more insight into $NF(X^3\Sigma^-)$ vibrational relaxation, modeling calculations have been carried out. The model treats only $\Delta v = 1$ collisional transfer, and the SF_6 rate constants of Table 1 were used as Reverse rate coefficients were calculated using the principle of detailed balance. $NF(X^3\Sigma^-)$ vibrational levels 0-3 were considered and were given an initial Boltzmann population distribution corresponding to a temperature of 2350 K, the nascent distribution observed in our experiments. The rate equations were numerically integrated to calculate time behavior of the $NF(X^3\Sigma^-)$ vibrational levels considered for a range of buffer gas densities.

buffer gas densities. The time profiles were fit in the same manner as the experimental data to obtain rise and decay rates. Plots of these rates as a function of buffer gas density were linear, and Table 2 displays the results. Three separate sets of modeling calculations were performed at three different temperatures, affecting the reverse rate constants, $k_{v \to v+1}$, through detailed balance. It should be noted that in all three cases, the initial $NF(X^3\Sigma^-)$ vibrational distribution was held constant. As expected, the rate constants obtained from fitting the simulated data are nearly identical to those used as input to the model at the lowest temperature, -100°C, while those from the highest temperature, 1000°C, deviate significantly. While not exact, there is good agreement between the model input rate coefficients and those determined from the calculation performed at our operating temperature of 144°C. This simulation of the experiment provides evidence that the data in Table 1 do indeed closely represent actual state-to-state vibrational transfer rate constants.

Classical models for vibrational energy transfer[24,25] predict that vibrational relaxation rate constants, $k_{v \to v-1}$, will scale with v for low vibrational levels. Such is the case with the CO_2 rate constants in Table 1, while the rate constants for SF_6 are seen to scale as v.[1,7] One could argue that the relatively inefficient quenching by CO_2 indicates that there is a weak interaction potential leading to more classical behavior, while a stronger interaction and deviation from classical behavior may be indicated by the larger SF_6 rate constants. However, quite the opposite is observed for HF,[26,29] where vibrational quenching by CO_2 is almost 3 orders of magnitude faster than quenching by SF_6. The efficient HF vibrational quenching by CO_2 has been attributed to the near resonant exchange $HF(v) + CO_2(00°0) \rightarrow HF(v-1) + CO_2(00°1)$.[30] No such near resonant channels exist for the case of NF(X) vibrational relaxation by CO_2. More modes are possible in SF_6, including the $\nu_4 + \nu_5$ combination band[31] at 1141 cm^{-1}. Although the probability for exciting a combination band is much lower than for single quantum exchange,[32] the resonance nature of this process must be noted [NF(X) $\omega_e x_e$ = 1141 cm^{-1}]. A suitable theoretical model that describes such processes has yet to be presented.[33]

Table 2. NF(X) Vibrational Relaxation Model Results[a]

k_{vv} Model Input	-100°C	144°C	1000°C
k_{10} 1.31×10^{-12}	1.12×10^{-12}[b]	1.12×10^{-12}[b]	1.05×10^{-12}[b]
k_{10} 1.31×10^{-12}	1.26×10^{-12}[c]	1.22×10^{-12}[c]	1.11×10^{-12}[c]
k_{21} 3.48×10^{-12}	3.36×10^{-12}	2.76×10^{-12}	1.26×10^{-12}
k_{32} 9.50×10^{-12}	9.50×10^{-12}	8.28×10^{-12}	2.08×10^{-12}

[a]All rate constants have units cm^3/molecule-sec. The initial $NF(X^3\Sigma^-)$ vibrational distribution used in the calculation was a Boltzmann distribution at a temperature of 2350 K.

[b]Rates obtained from the $v'' = 0$ risetimes.

[c]Rates obtained from the $v'' = 1$ decays.

B. NF($X^3\Sigma^-$) ROTATIONAL RELAXATION

The KrF laser photolysis of NF_2 also produces rotationally excited $NF(X^3\Sigma^-)$. An excitation spectrum of 0.25 Torr NF_2 and 0.75 Torr Ar, recorded with a 100 nsec delay between the excimer and dye lasers, is shown in Fig. 5 together with a plot of the normalized intensities of resolved lines in the NF b-X Q_p branch of the (0,0) band. An initial rotational temperature of 1750 K is obtained from the slope of the plot in Fig. 5. The time between NF-buffer gas hard-sphere collisions is about 170 nsec for the conditions under which the spectrum in Fig. 5 was recorded. Hence, the nascent $NF(X^3\Sigma^-)$ rotational distribution is well represented by these data. By monitoring the time behavior of selected rotational levels of the $NF(X^3\Sigma^-)$ state, we were able to obtain some information on rotational relaxation in the NF ground state. Since the rotational energy level spacing is about 2 orders of magnitude smaller than that for the vibrational levels, a state-to-state analysis analogous to that presented above is precluded. However, the investigation of the time evolution of the population in the lower rotational levels leads to phenomenological information on NF ground state rotational relaxation.

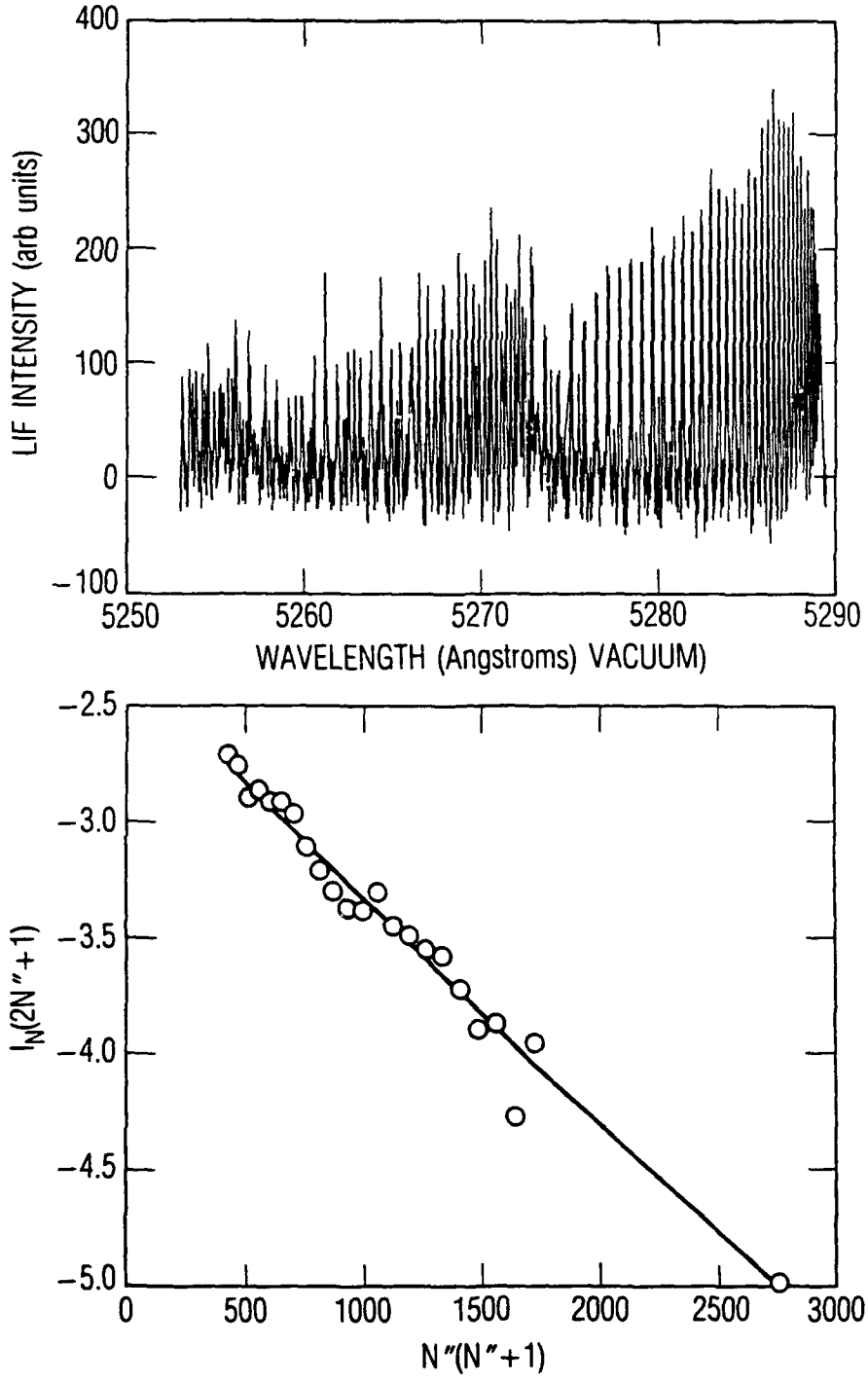

Fig. 5. Upper Trace: NF b-X Excitation Spectrum Taken from the KrF Photolysis of 0.27 Torr NF_2 and 0.75 Torr Ar. A delay of 100 nsec between the KrF laser and the dye laser was used. Visible are the (0,0) and (1,1) bandheads near 529 and 572 nm, respectively. Lower Trace: Intensities of the Resolved Lines in the Q_p Branch of the b-X (0,0) Band Plotted as a Function of the Rotational Quantum Number N". A rotational temperature of 1750 K is obtained from the linear fit indicated in the figure.

We monitored the laser-induced fluorescence (LIF) from probing the N"=9 level of the NF($X^3\Sigma^-$) v"=2 vibrational level as a function of CO_2 pressure. Figure 6 displays time profiles for this level with and without CO_2. The population in N"=9, near the maximally populated level at our cell temperature of 420 K ($N"_{max}$ = 10), is observed to increase as a function of time. This is a consequence of the rotational equilibration of the v"=2 rotational manifold as population funnels down from the higher N" levels initially populated following NF_2 dissociation. The v"=2, N"=9 inverse risetime is plotted versus CO_2 density in Fig. 7. A lack of knowledge of the mechanism of rotational relaxation in NF(X) prevents extraction of any detailed information from the data in Fig. 7. The slope of the plot, 4.4×10^{-11} cm^3/molecule-sec, represents an empirical rate constant which describes how the rotational manifold is relaxed by CO_2 from its initial distribution of 1750 K to a distribution at our cell temperature. At the initial temperature of 1750 K, N_{max} is 22, and hence the relaxation process observed must occur over a number of collisions since large ΔN collisions are decreasingly probable.[34-36] Thus, state-to-state rotational transfer rate constants for NF(X) are probably several times larger than this number for small ΔN processes. This seems reasonable considering rates of other species studied.[34-40] It is interesting to note that the intercept of the plot of Fig. 7 yields an empirical rate constant for Ar which agrees within experimental error with that for CO_2. The v"=0 level of NF(X) was also investigated, and the rate constants for N"=9 are equal to those for v"=2. If the mechanism for relaxation is the same for v"=0 and v"=2, we can conclude that no vibrational dependence for rotational relaxation is observed.

C. REMOVAL OF NF($X^3\Sigma^-$)

Through computer modeling of experimental H and N atom profiles observed from the reaction of NF_2 with hydrogen atoms, Cheah et al.[5] concluded that the bimolecular disproportionation of NF is rapid, $k = 7 \times 10^{-11}$ cm^3/molecule-sec, and is the predominant decay channel:

$$NF + NF \rightarrow N_2 + 2F \qquad (1)$$

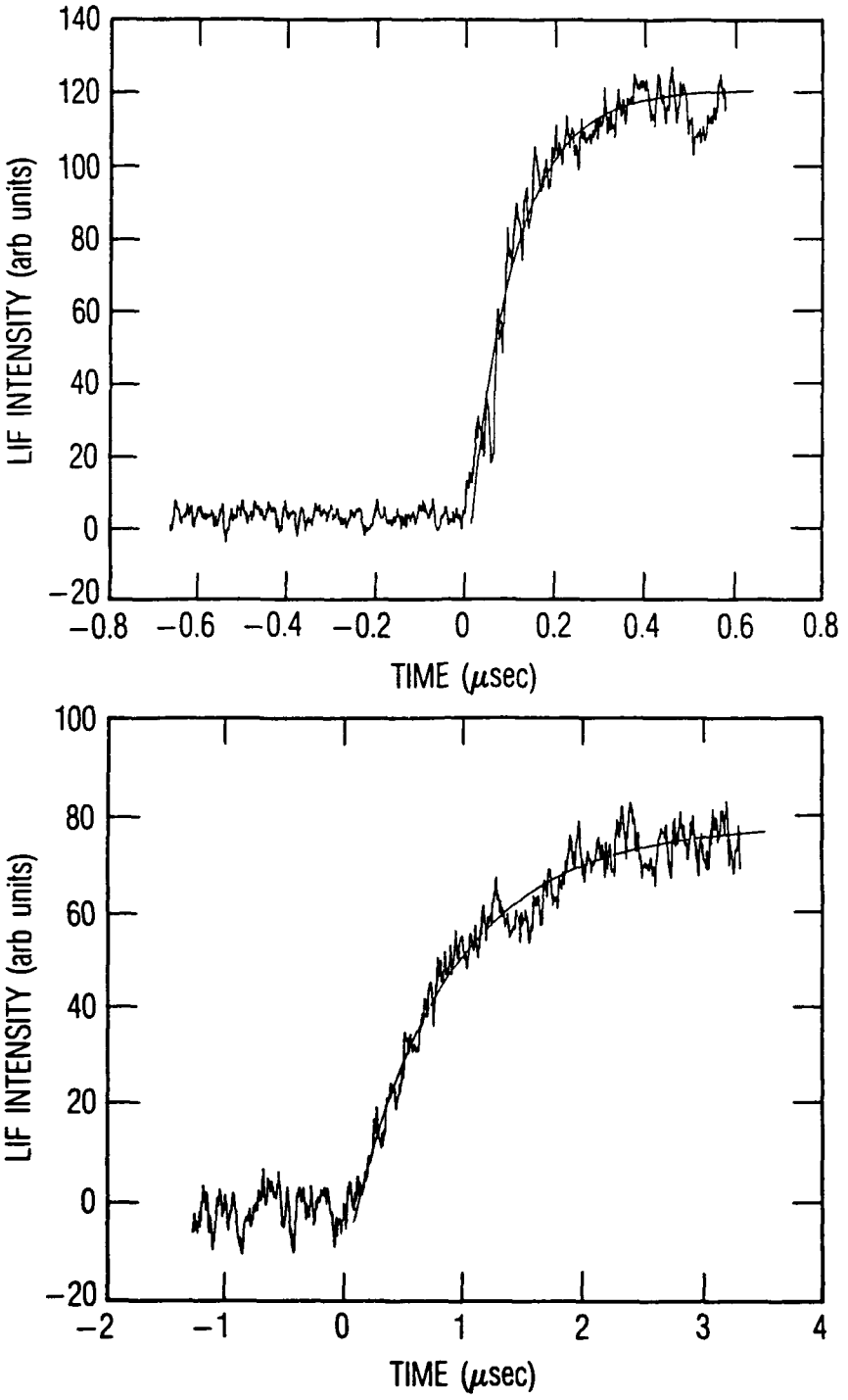

Fig. 6. Time Profiles of the v"=2, N"=9 Level of NF(X) Showing Rotational Equilibration. The NF_2 and Ar partial pressures are 0.25 and 1.3 Torr, respectively. The upper trace shows the behavior with a CO_2 partial pressure of 8.4 Torr, while the lower curve shows the time profile with no added CO_2. Note the difference in the time scales. A single exponential fit to the data is also shown.

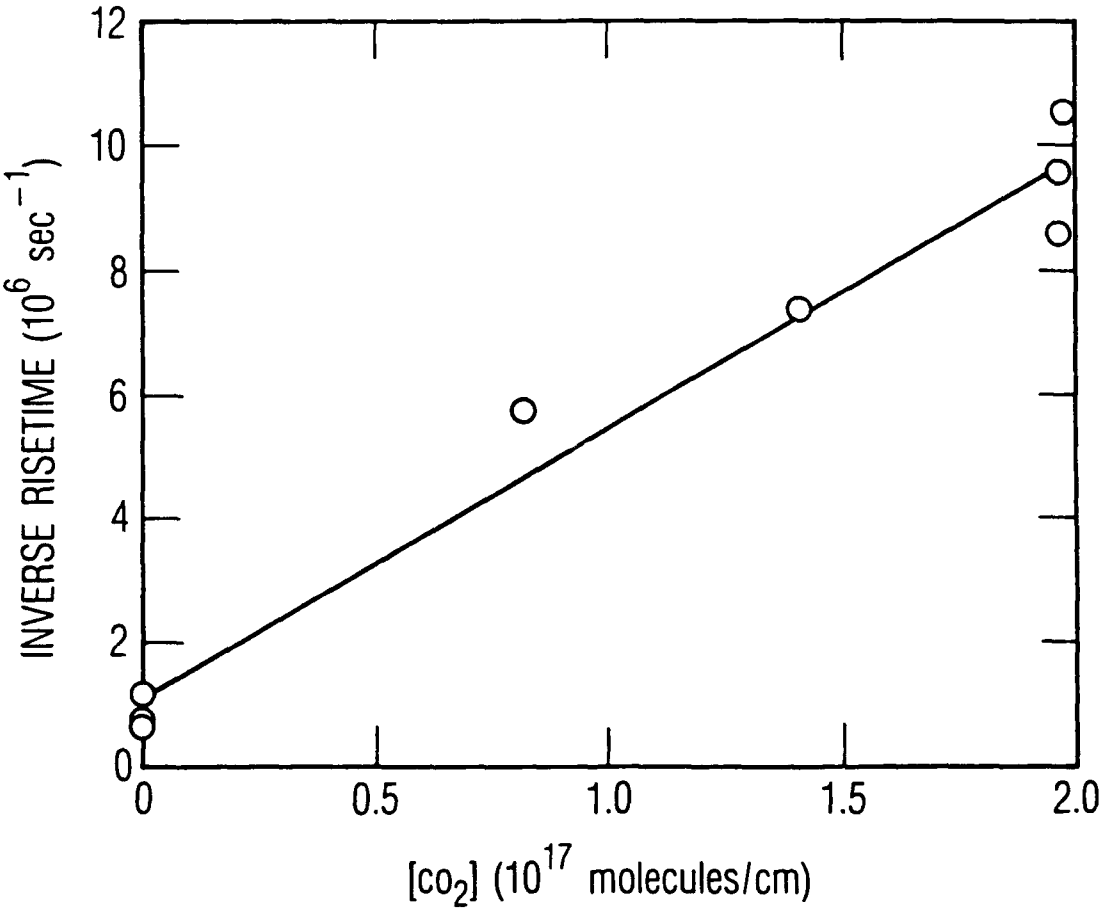

Fig. 7. Rise rate of NF(X), v"=2, N"=9 Plotted vs CO_2 Density. The squares are the experimental data and the solid line is a linear fit. The slope of the line is 4.4×10^{-11} cm^3/ molecule-sec.

Their experiments were not state specific and only examined the overall removal rate of NF radicals. Previous work in this laboratory[8] has provided evidence that the NF(a) + NF(a) reaction is 3 orders of magnitude slower, $k \leq 1 \times 10^{-13}$ cm^3/molecule-sec. A more rapid rate was observed by Setser,[14] $k = 2 \times 10^{-12}$ cm^3/molecule-sec, still much slower than that reported in Ref. 5. The present technique permits direct measurement of the v"=0 level of NF($X^3\Sigma^-$) to determine its reaction kinetics. Experiments were carried out at a pressure of 14 Torr using SF_6 as the main buffer gas to ensure that rotational and vibrational equilibrium was rapidly attained in the NF($X^3\Sigma$) manifold. Figure 8 shows a representative time decay of NF($X^3\Sigma$) v"=0, N"=9. An experiment was performed that attempted to separate the second order disproportionation from the first order reaction of NF(X) with NF_2:

$$NF(X) + NF_2 \rightarrow N_2F_2 + F. \qquad (2)$$

If the expression for the removal rate of NF(X) is written as

$$k_r(sec^{-1}) = k_1[NF(X)] + k_2[NF_2] + k_d, \qquad (3)$$

we see that by holding $[NF(X)]_0$ and the total pressure constant, NF_2 can be varied to extract a rate coefficient for reaction (2). The constant k_d appearing in Eq. (3) is the diffusion rate of NF(X) out of the volume probed by the dye laser. The intercept would crudely represent the constant terms although process (1) is second order and a more complex kinetic expression must be employed in principle.

The results of a series of experiments in which the NF_2 density was varied are plotted in Fig. 9. The initial density of the NF(X) produced from the photolysis was held constant during these experiments by changing the KrF laser photolysis as the NF_2 concentration was changed. The NF($X^3\Sigma^-$) traces were well fit using a single exponential decay for the range of NF_2 and NF(X) densities used. The slope of a fit to the decays yields a rate constant for the reaction of NF($X^3\Sigma^-$) v"=0 with NF_2, whose

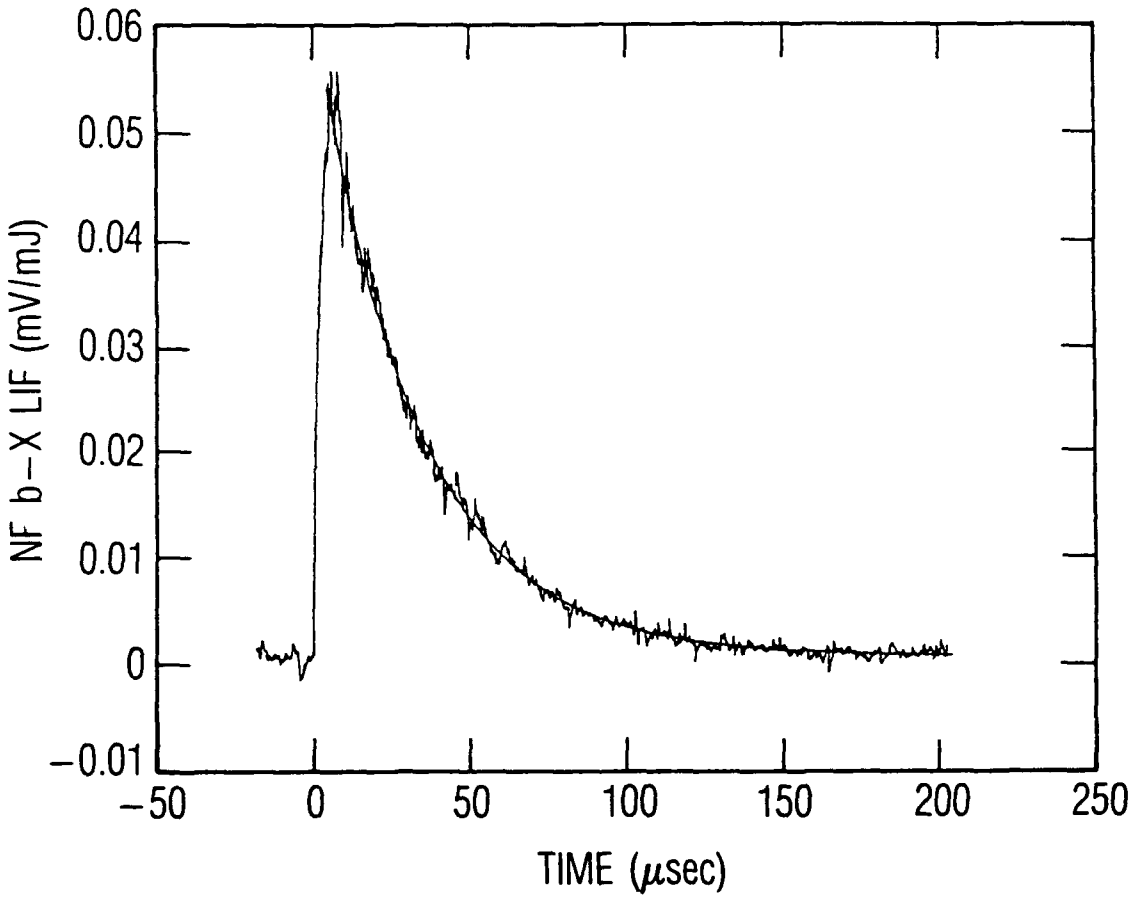

Fig. 8. Time Decay of NF(X), v"=0, N"=9 from the Photolysis of 0.62 Torr NF_2, 3.1 Torr Ar, and 11.9 Torr SF_6. The initial NF(X) produced from the photolysis is 7×10^{14} molecules/cm^3. Also shown is a single exponential fit to the decay.

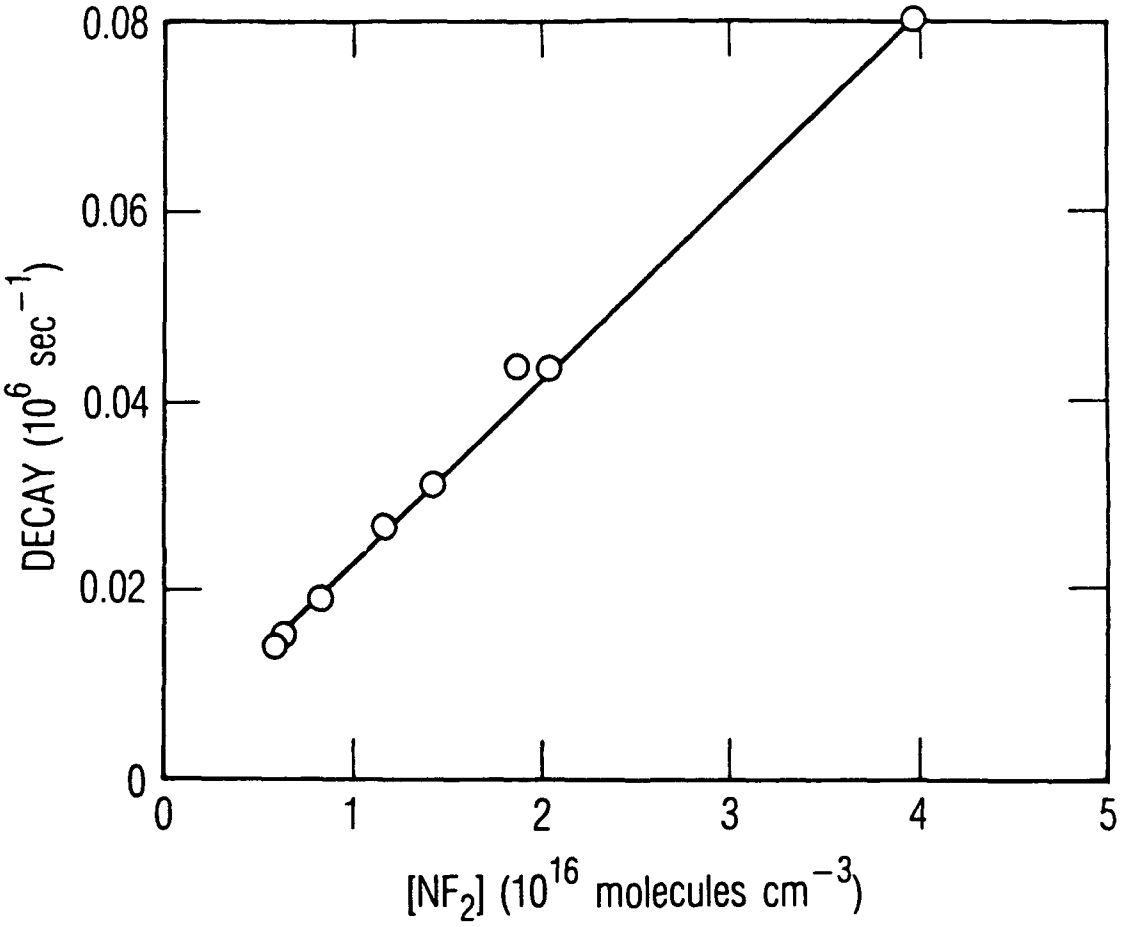

Fig. 9. Removal Rate of NF(X), v"=0, N"=9 as a Function of NF_2 Density. As the NF_2 density was increased, the KrF photolysis energy was decreased so that the fraction of the NF_2 photolyzed remained constant. The initial NF(X) density is 7×10^{14} molecules/cm^3. Also shown is a linear fit to the data. The slope of the fit is 2.0×10^{-12} cm^3/molecule-sec.

value is 1.97 ± 0.20 × 10^{-12} cm^3/molecule-sec. As noted, the intercept of the data of Fig. 9 contains information on $NF(X^3\Sigma^-)$ removal processes independent of NF_2. A knowledge of the KrF beam profile, determined from burn patterns and its energy, allows us to estimate an initial $NF(X^3\Sigma^-)$ density of 7 × 10^{14} molecules/cm^3 using the NF_2 absorption cross section at 249 nm[13]. Although diffusion coefficients for $NF(X^3\Sigma^-)$ are not known, we have calculated the diffusion time[41-43] of O_2 in Ar and SF_6 to estimate the role of diffusion in the present experiment. From the radial diffusion equation in a long cylinder,[44]

$$k_d = D_{12} (\pi^2/L^2 + 5.81/R^2), \qquad (4)$$

a radial diffusion rate of 1300 sec^{-1} is calculated for the conditions of this experiment [$D(O_2,Ar)$=0.30 cm^2/sec, $D(O_2,SF_6)$=0.22 cm^2/sec, R=0.25 cm, L=40 cm, and T=420 K]. This value is in reasonable agreement with the experimental intercept of 3000 ± 1500 sec^{-1} in Fig. 9. Under these conditions, the rate constant taken from Ref. 5 gives a second order $NF(X^3\Sigma^-)$ removal rate of (7 × 10^{-11}) × (7 × 10^{14}) = 4.9 × 10^4 sec^{-1}. If this were the case, we would expect the plot shown in Fig. 9 to deviate substantially from linear behavior at the lower NF_2 densities. In fact, no such behavior is observed. The plot is linear over the range of NF_2 studied and the intercept can be explained by diffusion alone. A simple kinetic model was constructed to obtain an estimate for the NF(X) second order removal rate constant. Reactions (1) and (2) were incorporated, and NF(X) was assumed to be in rotational and vibrational equilibrium. Figure 10 shows a comparison of the model results with the observed NF(X) decay at the highest initial NF(X) density attained. The calculated decay curve using disproportionation rate constant k_1 = 5 × 10^{-12} cm^3/molecule-sec lies considerably below the experimental data, while the model result with k_1 = 2 × 10^{-12} cm^3/molecule-sec is in reasonable agreement. Consideration of the data in Fig. 10 leads us to a conservative estimate that the $NF(X^3\Sigma^-)$ disproportionation rate coeficient is < 5 × 10^{-12} cm^3/molecule-sec.

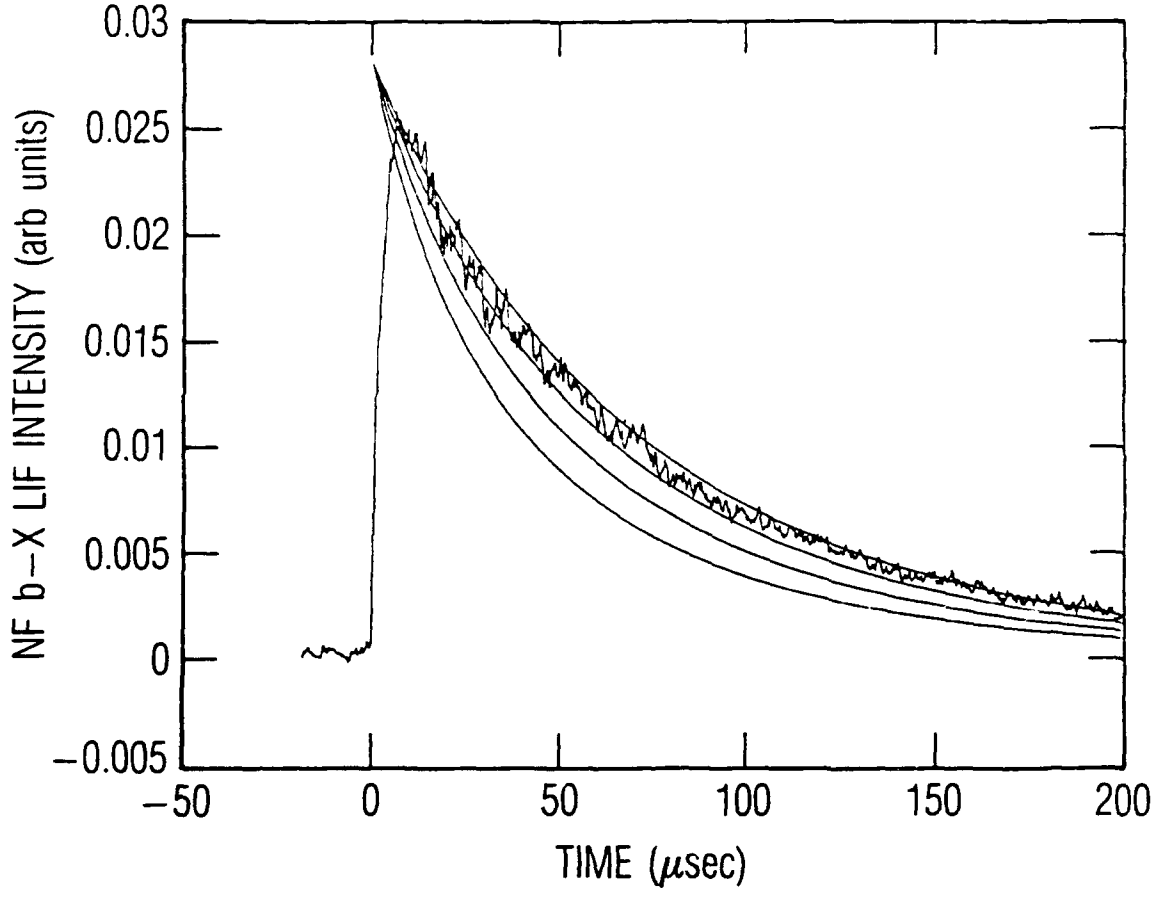

Fig. 10. Comparison of an Expermental NF(X), v"=0, N"=9 Decay Curve from the Photolysis of 0.31 Torr NF_2 in 11.6 Torr SF_6 and 1.0 Torr Ar with Model Calculations. The four smooth curves were calculated using an NF_2 + NF(X) rate constant of 2.0×10^{-12} cm^3/molecule-sec and four different values for the disproportionation rate constant (0.0, 2×10^{-12}, 5×10^{-12}, and 1×10^{-11} cm^3/molecule-sec).

IV. CONCLUSIONS

Vibrational relaxation of NF(X) produced from the 249 nm photolysis of NF_2 was investigated with CO_2 and SF_6 as the quenching partners. State-to-state vibrational quenching rate constants were obtained for NF(X, v" = 1-3). SF_6 is seen to be an efficient vibrational quencher of NF(X), while CO_2 is relatively inefficient, contrary to what is observed for HF vibrational relaxation. The equilibration rate of the nascent NF($X^3\Sigma^-$) rotational distribution (T_{rot} = 1750 K) has been studied and similar results were obtained for v"=0 and v"=2. The bimolecular disproportionation of NF(X) is seen to be much smaller than previously reported, while the reaction of NF(X) with NF_2 is surprisingly fast and may be the dominant removal mechanism for NF($X^3\Sigma^-$). The method used here has been applied to the determination of the branching ratio for the H + NF_2 → NF(X,a) + HF reaction and the results will be reported in a subsequent publication.

REFERENCES

1. a) J. M. Herbelin and N. Cohen, Chem. Phys. Lett. 20, 605 (1973).
   b) M. A. A. Clyne and I. F. White, Chem. Phys. Lett. 6, 465 (1970).

2. P. H. Tennyson, A. Fontijn, and M.A.A. Clyne, Chem. Phys. 62, 171 (1981).

3. J. M. Herbelin and R. A. Klingberg, Int. J. Chem. Kinet. 16, 849 (1984).

4. R. D. Coombe and A. T. Pritt Jr., Chem. Phys. Lett. 58, 606 (1978).

5. C. T. Cheah, M. A. A. Clyne, and P. D. Whitefield, J. Chem. Soc. Faraday Trans. II 76, 711 (1980).

6. C. T. Cheah and M. A. A. Clyne, J. Chem. Soc. Faraday Trans. II 76, 1543 (1980).

7. R. J. Malins and D. W. Setser, J. Phys. Chem. 85, 1342 (1981).

8. J. B. Koffend, C. E. Gardner, and R. F. Heidner III, J. Chem. Phys. 83, 2904 (1985).

9. P. B. Davies and W. J. Rothwell, Proc. R. Soc. Lond. A 389, 205 (1983).

10. D. E. Milligan and M. E. Jacox, J. Chem. Phys. 40, 2461 (1964).

11. A. C. Becker and U. Schurath, Chem. Phys. Lett. 142, 313 (1987).

12. D. Lin and D. W. Setser, J. Phys. Chem. 89, 1561 (1985).

13. H. Cha and D. W. Setser, J. Phys. Chem. 91, 3658 (1987).

14. E. Quinones, J. Habdas, and D. W. Setser, J. Phys. Chem. 91, 5155 (1987).

15. R. F. Heidner III, H. Helvajian, and J. B. Koffend, J. Chem. Phys. 87, 1520 (1987).

16. R. F. Heidner, H. Helvajian, J. S. Holloway, and J. B. Koffend (to be published).

17. F. A. Johnson and C. B. Colburn, J. Am. Chem. Soc. 83, 3043 (1961).

18. A. P. Modica and D. F. Hornig, J. Chem. Phys. 49, 629 (1968).

19. S. N. Foner and R. L. Hudson, J. Chem. Phys. 58, 581 (1973).

20. P. J. Evans and E. Tschuikow-Roux, J. Chem. Phys. 65, 4202 (1976).

21. P. J. Evans and E. Tschuikow-Roux, J. Phys. Chem. 82, 182 (1978).

22. A. E. Douglas and W. E. Jones, Can. J. Phys. 44, 2251 (1966).

23. M. Vervloet and J. K. G. Watson, Can. J. Phys. 64, 1529 (1986).

24. E. W. Montroll and K. E. Schuler, J. Chem. Phys. 26, 454 (1957).

25. R. C. Millikan and D. R. White, J. Chem. Phys. 39, 3209 (1963).

26. J. F. Bott, J. Chem. Phys. 65, 4239 (1976).

27. P. R. Poole and I. W. M. Smith, J. Chem. Soc. Faraday Trans. II 73, 1434 (1977).

28. R. D. H. Brown, D. J. Douglas, and J. C. Polyanyi, J. Chem. Soc. Faraday Trans. II 75, 422 (1979).

29. J. F. Bott and N. Cohen, J. Chem. Phys. 61, 681 (1974).

30. R. R. Stephens and T. A. Cool, J. Chem. Phys. 56, 5683 (1972).

31. T. Shimanouchi, Tables of Molecular Vibrational Frequencies, NSRDS-NBS 39 (1972).

32. Y. T Yardley and C. B. Moore, J. Chem. Phys. 46, 4491 (1967).

33. L. S. Dzelzkalns and F. Kaufman, J. Chem. Phys. 81, 4975 (1984).

34. R. A. Copeland and F. F. Crim, J. Chem. Phys. 78, 5551 (1983).

35. P. Brechignac, Opt. Commun. 25, 53 (1978).

36. J. J. Hinchen and R. H. Hobbs, J. Chem. Phys. 65, 2732 (1976).

37. T. A. Brunner, N. Smith, A. W. Karp, and D. E. Pritchard, J. Chem. Phys. 74, 3324 (1981).

38. R. K. Lengel and D. R. Crosley, J. Chem. Phys. 67, 2085 (1977).

39. J. A. Barnes, M. Keil, R. E. Kutina, and J. C. Polanyi, J. Chem. Phys. 76, 913 (1982).

40. P. J. Dagdigian and M. H. Alexander, J. Chem. Phys. 72, 6513 (1980).

41. S. D. Hamann, W. J. McManamey, and J. F. Pearse, Trans. Farad. Soc. 49, 351 (1953).

42. M. Trautz, A. Melster, and R. Zink, Ann. Physik(5) 7, 409 (1930).

43. E. Whalley and W. G. Schneider, J. Chem. Phys. 23, 1644 (1955).

44. R. J. Donovan and D. Husain, Adv. Photochem. 8, 1 (1974).